Shear waves over longshore nonuniform barred beaches

F.E. Sancho[1] and I.A. Svendsen[2]

Abstract

In the present paper we address the far-infragravity motion (0.001–0.01 Hz) associated with shear (or vorticity) waves over a fixed-bed, longshore nonuniform beach. The model equations are simplified forms of the fully nonlinear, depth-integrated, wave-averaged Reynolds equations, which are solved by the SHORECIRC numerical model. The currents are forced by stationary, monochromatic, incident short waves. The formation of flow instabilities depends on physical model parameters (e.g., bottom friction), the incident wave field, and the beach topography. The latter two effects are analysed here in the prediction of shear waves and unsteady rip-currents.

1 - Introduction

Shear waves were first observed in the field by Oltman-Shay *et al.* (1989), and were recognized by Bowen and Holman (1989) as instabilities of the longshore currents. The latter authors analysed the dynamics of these motions over a simple geometry for the linear and frictionless system of equations governing the perturbed velocities. Other analytical and numerical studies included the effect of bottom shear stresses and lateral turbulent mixing, and extended the analysis to planar and barred longshore uniform beaches (Putrevu and Svendsen, 1992b; Dodd *et al.*, 1992; Allen *et al.*, 1996; Özkan-Haller and Kirby, 1996). These studies gave insight into the shear wave dynamics, and comparisons with field data (collected during the SUPERDUCK experiment) showed a good agreement of the predicted versus the observed range of frequencies and wavelengths at which these motions were strong.

[1]Laboratório Nacional de Engenharia Civil, Av. do Brasil, 101, 1799 Lisbon, Portugal. E-mail: fsancho@lnec.pt

[2]Center for Applied Coastal Research, University of Delaware, Newark, DE 19716, USA. E-mail: ias@coastal.udel.edu

The studies mentioned above, however, only considered a longshore uniform beach. The problem studied here deals with the effect that the longshore variation of the topography has on the development of shear waves. Sinusoidally longshore varying topographies have been considered in the analysis of shear waves by Deigaard *et al.* (1994) and Slinn *et al.* (1996). The results of the former suggest that growing amplitudes of the longshore bottom disturbances act to suppress the shear instabilities of the background flow. In another example, Sancho *et al.* (1997) showed model predictions of shear instabilities over a surveyed bathymetry at Duck, North Carolina. The beach was characterized by the presence of an almost uniform longshore bar.

In the present paper we isolate and study the effect of well-defined longshore bottom variations on the characteristics of the shear instabilities. The goal is to analyze the nonlinear evolution of shear (vorticity) instabilities over canonical longshore varying, fixed bed, beach configurations. Hence, we look at the influence of rip-channels in the mean and time-varying (unstable) flow field.

2 - Model equations and numerical method

In this study we make use of the depth-integrated, short-wave averaged Reynolds equations. We assume turbulent flow, but neglect the turbulent normal stresses, and we also assume zero surface shear stress. For depth-varying currents the governing equations for conservation of mass and momentum can be written in Cartesian coordinates ($(x, y, z) \equiv (x_\alpha, z)$ in tensor notation) as (e.g., Van Dongeren *et al.*, 1994):

$$\frac{\partial \bar{\zeta}}{\partial t} + \frac{\partial \bar{Q}_\alpha}{\partial x_\alpha} = 0\,, \tag{1}$$

$$\frac{\partial \bar{Q}_\beta}{\partial t} + \frac{\partial}{\partial x_\alpha}\int_{-h_o}^{\bar{\zeta}} V_\alpha V_\beta \, dz + \frac{\partial}{\partial x_\alpha}\overline{\int_{\zeta_t}^{\zeta} (u_{w\alpha} V_\beta + u_{w\beta} V_\alpha)\, dz} =$$

$$-g\,(h_o + \bar{\zeta})\frac{\partial \bar{\zeta}}{\partial x_\beta} - \frac{1}{\rho}\frac{\partial}{\partial x_\alpha}\left[S_{\alpha\beta} - \overline{\int_{-h_o}^{\zeta} \tau_{\alpha\beta}\, dz}\right] - \frac{\tau_\beta^B}{\rho}\,. \tag{2}$$

In these equations $\bar{\zeta}$ is the mean surface elevation, h_o is the still water depth, and ρ is the fluid density. $\tau_{\alpha\beta}$ represents the turbulent shear stress tensor, V_α is the horizontal current velocity and $\bar{Q}_\alpha$ is the depth-integrated volume flux, defined as

$$\bar{Q}_\alpha = \int_{-h_o}^{\bar{\zeta}} V_\alpha \, dz + Q_{w\alpha}\,, \tag{3}$$

where $Q_{w\alpha}$ is the shortwave-induced mean volume flux. In equation (2), $u_{w\alpha}$ is the short-wave velocity component, $S_{\alpha\beta}$ is the radiation stress tensor (defined according to Mei, 1989), and the bottom shear stress is represented by τ_α^B.

The system of equations above constitute the basis of the Quasi-3D numerical model SHORECIRC (Van Dongeren *et al.*, 1994). A somewhat simplified version of that model is used here.

The turbulent shear stress (the turbulent lateral mixing) is modeled according to the eddy viscosity closure, assuming that

$$\tau_{\alpha\beta} = \rho \nu_t \left(\frac{\partial V_\alpha}{\partial x_\beta} + \frac{\partial V_\beta}{\partial x_\alpha} \right) , \tag{4}$$

where the eddy viscosity ν_t is calculated by (Sancho and Svendsen, 1997)

$$\nu_t = C_1 \kappa \sqrt{\frac{f_w}{2}} u_0 h + M h (\frac{D}{\rho})^{1/3} . \tag{5}$$

The first term of equation (5) represents the bottom-induced turbulence and it is always present (Coffey and Nielsen, 1984), whereas the second term accounts for the turbulence generated by the breaking waves (Battjes, 1975), and it is only active in the surf region. In the above, D is the energy dissipation rate per unit area, M and C_1 are constants, κ represents the von Karman constant, f_w is the bottom friction coefficient, and u_0 is the amplitude of the short-wave orbital velocity at the bottom. We choose $M = 0.1$, which is one order of magnitude smaller than the value suggested by Battjes (1975), because it gives estimates of ν_t in agreement with those estimated by Svendsen (1987). Similary we choose $C_1 = 0.75$, which yields values of ν_t outside the surf region of the same order as the experimental results of Cox *et al.* (1995).

The shortwave-averaged bottom shear stress is computed according to the nonlinear wave-current formulation of Putrevu and Svendsen (1992a),

$$\tau_\alpha^B = \frac{1}{2} \rho f_w u_0 (\beta_1 V_\alpha + \beta_2 u_{0\alpha}) , \tag{6}$$

where β_1 and β_2 depend on the short-wave phase angle, and the current and short-wave orbital velocity magnitude and direction. The friction factor is chosen as $f_w = 0.006$. The orbital velocity amplitude u_0 is calculated according to linear wave theory, and the energy dissipation rate D is given by Dally *et al.* (1985), with the wave field obtained from REF/DIF1 (Kirby and Dalrymple, 1994) model applications. The results from this model (wave height and direction) are also used to estimate the radiation stress $S_{\alpha\beta}$, and the wave-induced volume flux $Q_{w\alpha}$, using linear wave theory. Inside the surfzone, an extra term has been added to $Q_{w\alpha}$ in order to account for the effect of the mass of water transported shorewards by the roller (Svendsen, 1984).

The system of equations above is solved numerically by a third-order ($\mathcal{O}(\Delta t^3)$) predictor-corrector finite difference method. Spatial derivatives are 4th-order accurate (Sancho and Svendsen, 1997). The (horizontal) domain of integration is discretized by a rectangular grid with open boundaries everywhere, except at the shoreline. At the seaward boundary, a generating-absorbing condition is used (Van Dongeren and Svendsen, 1997), and at the shore-normal boundaries a periodicity condition is implemented. At the landward boundary, the shoreline (horizontal) position is held fixed with the boundary condition $V_\alpha = 0$ at a small water depth ($\sim 0.005 - 0.05$ times the water depth at breaking, h_b). We note that a similar treatment of the shoreline is utilized by Özkan-Haller and Kirby (1997), as those authors found minor differences between the results obtained by including the shoreline runup and those from calculations with a zero-velocity condition at the shore.

3 - Applications

3.1 - Longshore uniform plane beach

Although most natural beaches can exhibit complicated bottom contours, it is interesting to analyze the development and propagation of shear waves on a longshore uniform plane beach. We choose to first investigate the nonlinear shear instabilities on a 1/20 sloping beach with the same characteristics as that studied by Allen *et al.* (1996) and Özkan-Haller and Kirby (1995, 1997). We also use this example to test the numerical accuracy of our model versus the accuracy of the different numerical schemes of those other models.

Hence for the purpose of the comparison, we assume the currents are depth uniform. We also consider a longshore uniform beach and assume the short-wave forcing in the cross-shore direction to be in balance with the setup gradient, and in the longshore direction it balances the bottom shear stress associated with the steady (time-averaged over the infragravity oscillations) longshore current V_S and the lateral mixing (see above references and Sancho and Svendsen, 1997, for details). This implies that the lateral mixing from turbulence and the mixing effects of the nonlinear intergrals in (2) are included for the V_S-part of the total velocity. However, we neglect turbulent and dispersive mixing effects generated by the deviations in the velocity from V_S. Similarly (6) is linearized so that the bottom shear stresses are linear functions of U and V

$$\tau_x^B = \rho\,\mu\,U\,, \tag{7}$$

$$\tau_y^B = \rho\,\mu\,(V - V_S)\,, \tag{8}$$

with a constant friction coefficient $\mu = 0.006$. This essentially reduces the complete equations to the model equations of Özkan-Haller and Kirby (1997). Those are a slightly modified set of the equations solved by Allen *et al.* (1996), who further introduced the rigid lid approximation. Initial and boundary conditions are also similar to those of the authors above.

The longshore domain length l_y equals that of the most unstable wavelength calculated from linear instability theory, $l_y = 5x_b'$, where $x_b' = 90$ m is the distance from the shoreline to the position of the maximum of the longshore current. In the cross-shore direction the domain length is $l_x = 4x_b'$. The grid spacings are the same as those used by Allen *et al.*, namely $\triangle x = \triangle y = \frac{x_b'}{18} = 5$ m.

Fig. 1 shows the time series of $\eta, \tilde{U}$ and $\tilde{V}$ at $\frac{x}{l_x} = 0.75$ and $\frac{y}{l_y} = 0.5$, predicted both by the present model (upper three panels) and the numerical model of Özkan-Haller and Kirby (1997) (lower three panels). The landward-oriented cross-shore direction with origin at the seaward domain boundary is denoted by x. For both model results, we see that the amplitude of the shear waves grows quasi-exponentially for $2-3.5$ hr, and then remains quasi-steady, oscillating around a mean value. It is also visible that the higher amplitude disturbances have larger periods, which confirms previous observations on the weakly dispersive properties of shear waves (Oltman-Shay *et al.*, 1989). Although they differ in some details, the similarity between our results and

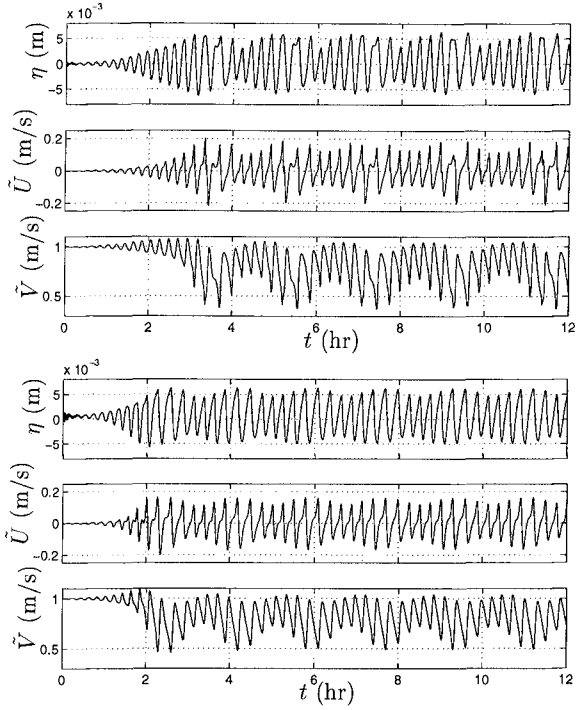

Figure 1: Time series of $\eta, \tilde{U}$ and $\tilde{V}$ at $\frac{x}{l_x} = 0.75$ and $\frac{y}{l_y} = 0.5$ from the present model simulations (upper three plots) and Özkan-Haller and Kirby (1997) model simulations (lower three plots).

those of Özkan-Haller and Kirby is evident. We have also compared the present solution with that of Allen *et al.* (1996), and the agreement is not quite as good, which may be due to the rigid-lid assumption of Allen *et al.*. For brevity the results are omitted here.

Analysis of the results also shows that the shear wave propagation velocity c_S is within the interval $0.5 < \frac{c_S}{V_M} < 0.54$, where V_M is the maximum of the initial longshore current profile. The low-frequency oscillations ($T \simeq 2$ hr) are the same in ours and Özkan-Haller and Kirby's results.

It is interesting to analyze the effect the shear wave motion produces on the mean longshore current. The initial current forms a quasi longshore uniform flow with the longshore current profile as plotted in Fig. 2. However, the shear waves cause a dispersion of momentum, which will modify the background time-mean longshore current profile relative to the profile maintained by the forcing and turbulent mixing. This is illustrated in Fig. 2, where we plot the initial cross-shore profile of the longshore current at $\frac{y}{l_y} = 0.5$ (solid line), versus the current profile obtained by time-averaging V over the entire period of simulation ($t = 12$ hr), (dashed line). The maximum of

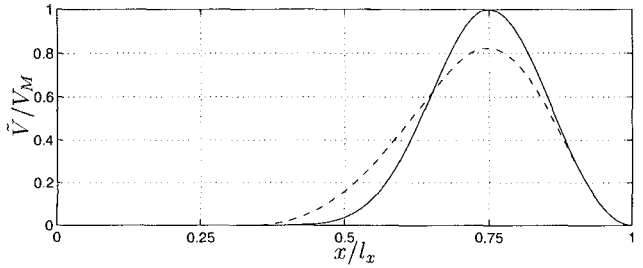

Figure 2: Cross shore distribution of the initial (——) and time-averaged (- -) longshore current over a longshore uniform plane beach.

the time-averaged longshore current is approximately 20% smaller than that of the initial distribution. this result is similar to the results of Özkan-Haller and Kirby (1997).

3.2 - Longshore varying barred beach

Weak longshore forcing gradient

As a second example we analyze the nearshore currents over a periodically longshore varying barred beach. The longshore bottom perturbation is characterized by a slight depression in the bar crest, similar to the formation of a rip-channel (Fig. 3), located at the centerline of the computational domain. The bottom topography used in the present example is similar to the barred beach often encountered at the FRF experimental station in Duck, NC (e.g., Thornton and Kim, 1993). Details of the analytical expression for the bathymetry are given by Sancho and Svendsen (1997). The governing equations, closure submodels, and relevant parameters are given by equations (1)–(6). For simplicity and brevity, we again consider (below-trough) depth-uniform currents only. It turns out that the dispersive mixing caused by depth varying currents will somewhat reduce the development of the shear waves. This more complex situation was analysed in Sancho and Svendsen (1997). The initial condition for the simulations is a "cold start", and the short-wave forcing is "ramped" smoothly until it reaches a steady forcing.

The relevant parameters that define the bathymetry and domain size are the crest to shoreline distance $l_c = 120$ m, and the domain lengths in the cross-shore and longshore directions, $l_x = 4\,l_c$, and $l_y = 16\,l_c$, respectively. The depth at the crest of the longshore uniform section of the bar is $h_c \simeq 1.18$ m, and at the rip-channel is just 10% deeper. The width of the rip-channel is $w_r = 0.84\,l_c$ (100 m), and the numerical grid spacings are $\triangle x \simeq 4.24 h_c$ (5 m) and $\triangle y \simeq 8.48 h_c$ (10 m).

First, we choose the incident wave conditions so that intense wave breaking occurs

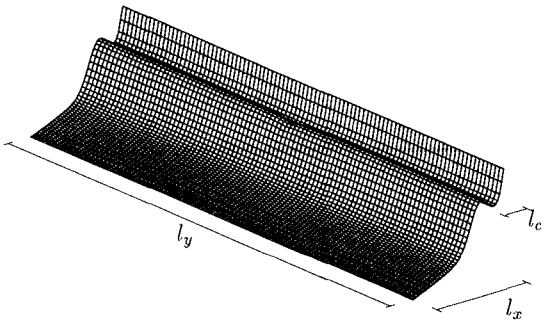

Figure 3: Perspective view of the barred beach for the example in section 3.2.

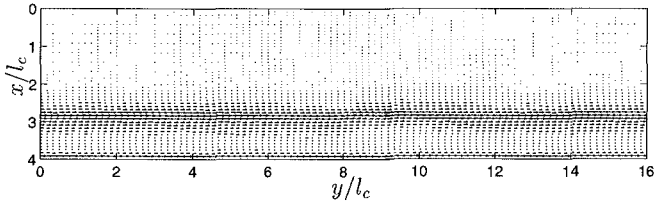

Figure 4: Time-averaged (over 4 hr), depth-averaged, current velocity vectors for the case of weak longshore forcing gradient.

along the entire bar, including over the rip channel, starting just before the bar crest, (at $x/l_c = 2.75$). The waves then propagate over the bar-trough without breaking before a second breaking occurs nearer the shoreline. This results in a nearly longshore uniform wave forcing. In numbers, the wave height at the seaward boundary ($x = 0$) is $H_o = 0.9\,h_c$ (1.06 m), the incident wave angle is $\alpha_{w0} = 7.5°$ with the shore normal direction x, the wave period is $T = 14.4\sqrt{h_c/g}$ (5 s), and the breaking criterion $H_b/h_b = 0.78$ is used.

Time-averaged velocity vectors of the current field are shown in Fig. 4. The time-averaging is performed over a period of approximately 4 hr, after the flow reached near stationarity. The time-averaged velocity vectors show a slight variation of the flow at the region of the rip-channel ($y = 8\,l_c$). The largest variations are observed, as expected, around the rip-channel, but are more pronounced slightly downstream of it due to the inertia of the flow. In fact, examination of the magnitude of the terms in the longshore momentum equation shows that it is a combination of a steady and a fluctuating component of the advective accelerations that are responsible for the divergence the flow around the rip-channel, and the existence of currents in the

trough, respectively. Away from the rip-channel it turns out that the wave-induced shoreward mass flux is locally balanced by the return current (undertow).

The results show that even a small rip-channel is able to disturb the otherwise longshore uniform flow, although, the existence of a rip-channel does not necessarily induce the formation of a rip-current. This turns out to be due to the fact that the wave field, as well as the mean surface elevation, are very homogeneous in the longshore direction. The (time-averaged) longshore current profile at any section exhibits the "classical" double-peaked distribution caused by the breaking over the bar and at the foreshore. There is, however, a significant current in the trough driven largely by the mixing generated by the shear waves.

The instantaneous nearshore current fields are, however, quite different from the time-averaged situation. Fig. 5 shows the instantaneous depth-averaged velocity vectors at four different times during the simulation. The first three pictures are at early stages of the computation, and show how the growth of shear waves starts at the rip-channel location. Looking consecutively at plots (a), (b) and (c) shear instabilities develop continuously at $y = 8\,l_c$, where the small channel is, and propagate downstream with the longshore current. In general, the shear wave celerity is equal to 0.45–0.65 of the maximum (time-averaged) longshore current, which is comparable to that suggested by field measurements (Dodd *et al.*, 1992). Between subplots (c) and (d) there is a significant time lapse (3.6 hr), during which the predicted predominant wavelength (and period) of the shear waves increased considerably. This frequency downshift is similar to that observed by Özkan-Haller and Kirby (1997). Closer inspection of the dynamics of these motions indicates that the shear waves are more intense seaward and over the bar-crest.

Clearly the rip channel acts as a strong disturbance that instantly initiates almost fully grown shear waves. Similar computations over a longshore uniform barred beach (not shown) indicate that shear waves develop much slower in the absence of the rip-channel. The longterm properties of the shear waves are, however, identical to those of the results just presented, indicating that once shear instabilities have formed they are relatively independent of small topographic perturbations.

Large longshore forcing gradient

The previous example illustrated that a nearly longshore uniform mean flow can occur over a longshore varying beach. In order to further analyse the conditions for generation of rip currents we consider an incident wave field that is slightly different from the previous example, over the same bottom topography of Fig. 3. The initial wave height is chosen so that outside the rip channel wave breaking occurs over the bar crest, whereas no breaking occurs in the rip-channel ($y = 8\,l_c$), (Fig. 6). The wave height is about 30% smaller at the seaward boundary than in the previous example. The incident wave angle and period are the same as before. The substantial differences in wave conditions over the rip-channel and the bar, induce strong longshore longshore variations of the forcing, in particular the pressure gradients. Note that although the wave model predictions may not be accurate, a similar trend in the wave height

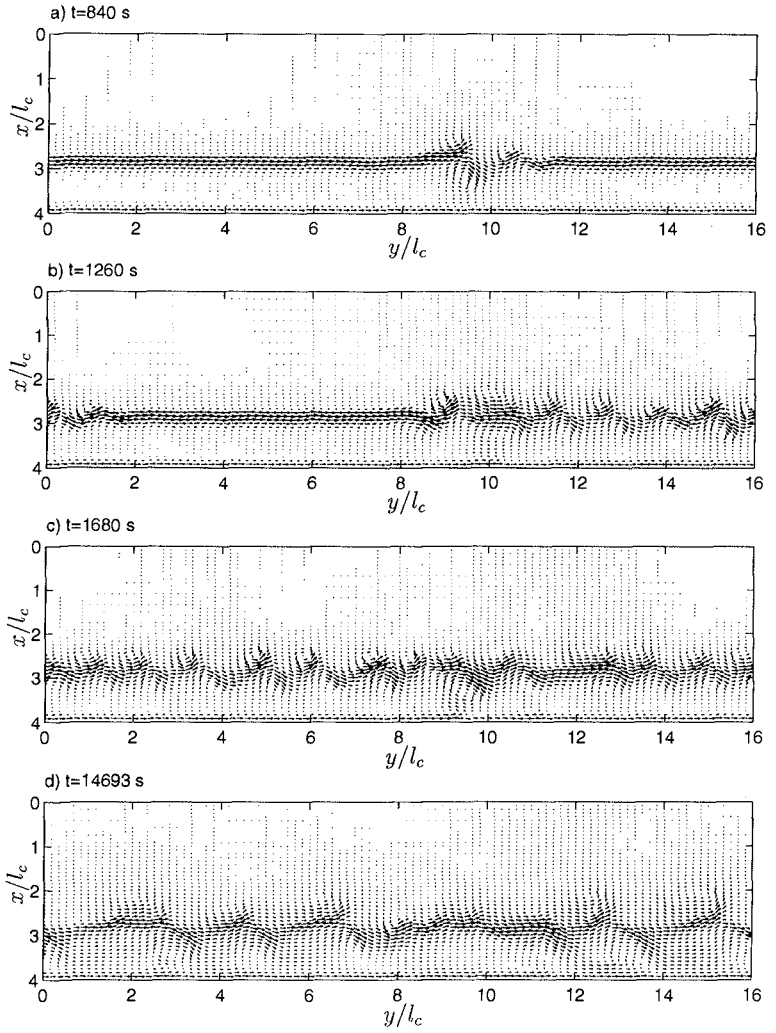

Figure 5: Depth-averaged current vectors at four instants of the simulation for the case of weak longshore forcing gradient.

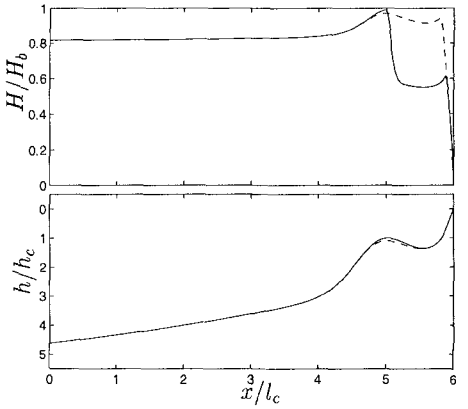

Figure 6: Wave height and bottom cross-shore variations over the barred beach at two longshore positions: $y = 0$ (solid line) and $y = 8\,l_c$ (dashed line) for the case of large longshore forcing gradient.

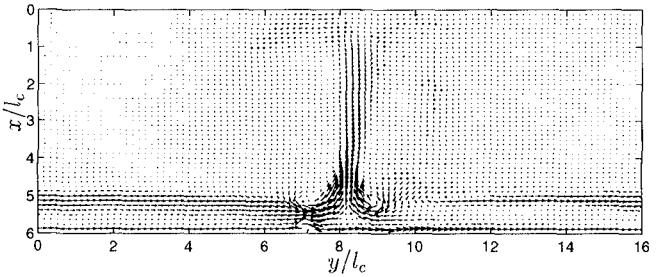

Figure 7: Time-averaged (over 2.1 hr), depth-averaged, current velocity vectors for the case of large longshore forcing gradient.

variation over the channel and the bar has been observed in laboratory experiments (Haller *et al.*, 1997).

The resulting time-averaged (over a period of 2.1 hr) and depth-averaged currents are illustrated in Fig. 7, which shows that a rip-current has formed, with two circulation cells around it, centered at the bar-crest. (The domain has been extended offshore to $l_x = 6\,l_c$). The width of the rip increases slowly towards offshore, as the result of a small turbulent dispersion as well as the dispersion caused by fluctuations of the rip (explained below). Bottom friction is also responsible for the widening of the rip. Longshore currents flow towards the rip-channel at both sides of the rip, mainly driven by local longshore gradients of the mean surface elevation. The maximum velocity in the rip-current is $0.2\sqrt{g\,h_c}$ (0.70 m/s), which is about twice as large as the maximum longshore current.

The results in Fig. 7 contrast with those of Fig. 4. Nearly longshore uniform currents are, however, found at a distance $10l_c$ (1200 m) from the channel axis.

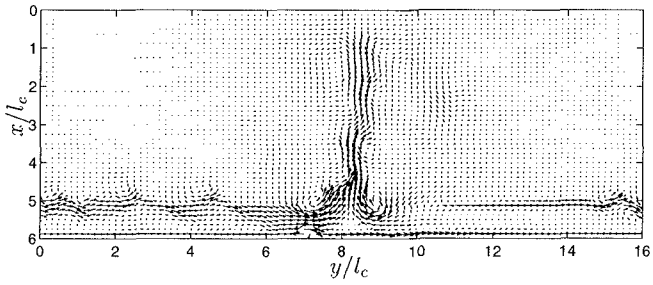

Figure 8: Instantaneous depth-averaged current vectors for the case of large longshore forcing gradient.

Larger differences from longshore uniformity mainly occur near and downstream of the rip-channel. Through inspection of the magnitude of the terms in the momentum equations, we find that the longshore pressure gradient and nonlinear advective accelerations are quite important in the longshore momentum balance, whereas in the cross-shore direction, the radiation stress gradient is mostly balanced by the surface elevation gradient.

The flow for the present simulation is, however, also unsteady. In fact, the current velocities are very dynamic, as can be seen in one "snapshot" of the depth-averaged current velocities, shown in Fig. 8. We find that in the rip-current vortices are generated at each side (note the similarity between the patterns predicted here and those observed in Fig. 7 of Shepard *et al.*, 1941). Initiation of shear wave motion is delayed. The motion is steady downstream of the rip-channel until $y = 14\,l_c$ and then shear waves start to form very rapidly over the longshore uniform section of the beach. Both the cross-shore and longshore velocities vary dramatically with the position, depending on whether this is located upstream or downstream of the rip-channel. We also see that shear waves approaching the rip channel from upstream are washed out to the sea by the rip current.

Inspection of the time series of the predicted velocities along the rip-channel indicates that the rip-currents are periodically unsteady. The most energetic periods of oscillation are seen to range between $400 < T < 450$ s, but there are also appreciable variations in the time series at a much lower frequency. The higher frequency oscillations are associated with a meandering motion of the rip-currents, whereas the longer period variations are related to a "side-to-side" shift of the rip-current, and with the passage of vortices released by the unstable rip over a certain location. Similarly, at locations where shear instabilities have formed, the period of the shear waves is initially ~ 440 s, and later a frequency downshift occurs and the period becomes ~ 800 s.

We find that the rip-current exhibits several features common with the shear waves. In fact, a hydrodynamic instability mechanism is common to the two flow types: shear waves are an instability mechanism of the longshore currents (Bowen and Holman, 1989), and rip-currents can be considered an unstable jet (whose me-

chanics are given by, e.g., Drazin and Reid, 1982). Both mechanisms have been observed in field and laboratory conditions, either isolated or simultaneously (e.g., Sonu, 1972). For the present conditions, the formation of the rip-current over the rip-channel destroys the structure and shear waves do not pass it.

Multiple rip-channels

Lastly, we investigated the effect of the domain size by performing calculations in a longshore periodic domain of size $l_y = \frac{10}{3} l_c$ (400 m) and $l_y = \frac{20}{3} l_c$ (800 m). Rip channels were 400 m apart, and the short-wave input lead to flow conditions similar to those of Figs. 4 and 5. This gave exactly the same longshore periodicity, and the results from these computations were identical, thus, meaning that the predicted shear waves were not dependent of the computational domain size. However, computations with different distance between the rip channels gave different patterns of the shear waves, with different period and wavelength, though their speed of propagation remained the same. Hence, the local signature of the shear waves appears to depend on the distance between rip-channels.

In a final example we chose a larger periodic domain size, of length $l_y = 1600$ m. Within this computational domain, we placed four rip-channels with different distances apart. The results from this computation showed the prediction of very irregular shear waves. In fact, time series of the predicted motions indicated a wide spectrum of energetic frequencies, which is in closer resemblance with those observed under field conditions (Oltman-Shay *et al.*, 1989). This suggests that the shear waves observed in nature may come from many different sources of disturbance.

4 - Conclusions

In this study we addressed the development of flow instabilities over longshore nonuniform barred beaches. It was found that shear waves can be triggered by small bottom perturbations (in the form of rip-channels) in an otherwise longshore uniform coast, but the shear wave average properties are nearly independent of these. Those properties are found to depend mainly of the background longshore current. Similarly, the distance between rip-channels also affects the shear waves dynamics.

A second important conclusion is that rip-currents not always form in the presence of rip-channels. Rip-currents may occur when short-wave conditions give rise to large longshore forcing gradients around the rip-channel such as changes in breaking conditions. In that situation, unstable rip-currents were predicted. Conversely, shear waves can be suppressed by the existence of rip-currents, and will then form far downstream of the rip-channel, seemingly away from the influence of the rip.

The results suggest that the longshore variability of a beach, over a considerable domain length, can play an important role in the prediction of the dynamics of steady and unsteady currents. Hence, care should be taken in the comparison of model to field results, when assuming longshore uniform conditions, or using too small model domains.

Acknowledgments

Funding was provided by the Office of Naval Research, Coastal Sciences, (contract no. N00014-95-C-0075). The first author held a scholarship from the Portuguese Research Council (PRAXIS XXI, contract no. BD/3656/94). The U.S. Government is authorized to produce and distribute reprints for government purposes notwithstanding any copyright notation that may appear herein.

References

Allen, J., P. A. Newberber, and R. A. Holman (1996). Nonlinear shear instabilities of alongshore currents on plane beaches. *J. Fluid Mech.* (310), 181–213.

Battjes, J. A. (1975). Modeling of turbulence in the surf zone. In *Proc. Symp. on Modelling Techniques*, San Francisco, 1050–1061.

Bowen, A. J. and R. A. Holman (1989). Shear instahilities in the mean longshore current: 1-theory. *J. Geophys. Res. 94*(C12), 18023–18030.

Coffey, F. C. and P. Nielsen (1984). Aspects of wave current boundary layer flows. In *Proc. 19th Int. Conf. Coastal Engng.*, Vol. 3, Houston, 2232–2245. ASCE.

Cox, D. T., N. Kobayashi, and A. Okayasu (1995). Experimental and numerical modeling of surf zone hydrodynamics. (Ph. D. Dissertation) Res. Report CACR-95-07, Center for Applied Coastal Research, Univ. of Delaware.

Dally, W. R., R. G. Dean, and R. A. Dalrymple (1985). Wave height variation across beaches of arbitrary profile. *J. Geophys. Res. 90*(C6), 11917–11927.

Deigaard, R., E. D. Christensen, J. S. Damgaard, and J. Fredsœ(1994). Numerical simulation of finite amplitude shear waves and sediment transport. In *Proc. 24th Int. Conf. Coastal Engng.*, Vol. 2, Kobe, 1919–1933. ASCE.

Dodd, N., J. Oltman-Shay, and E. B. Thornton (1992). Shear instahilities in the longshore current: A comparison of observation and theory. *J. Phys. Oceanogr. 22*(1), 62–82.

Drazin, P. G. and W. H. Reid (1982). *Hydrodynamic stability.* Cambridge: Cambridge University Press. pp. 527.

Haller, M. C., R. A. Dalrymple, and I. A. Svendsen (1997). Rip channels and nearshore circulation. In *Coastal Dynamics'97*, Plymouth, 594–603. ASCE.

Kirby, J. T. and R. A. Dalrymple (1994). Combined refraction/diffraction model REF/DIF1, Version 2.5. Res. Report CACR-94-22, Center for Applied Coastal Research, Univ. of Delaware.

Mei, C. C. (1989). *The Applied Dynamics of Ocean Surface Waves.* Singapore: World Scientific. pp. 740.

Oltman-Shay, J., P. A. Howd, and W. A. Birkemeier (1989). Shear instabilities in the mean longshore current: 2-field observations. *J. Geophys. Res. 94*(C12), 18031–18042.

Özkan-Haller, H. T. and J. T. Kirby (1995). Finite amplitnde shear wave instabilities. In *Coastal Dynamics'95*, Gdansk, 465–476. ASCE.

Özkan-Haller, H. T. and J. T. Kirby (1996). Numerical study of low frequency surf zone motions. In *Proc. 25th Int. Conf. Coastal Engng.*, Vol. 2, Orlando, 1361–1374. ASCE.

Özkan-Haller, H. T. and J. T. Kirby (1997). Nonlinear evolution of shear instabilities of the longshore current. (Ph. D. Dissertation), Res. Report CACR-97-08, Center for Applied Coastal Research, Univ. of Delaware.

Putrevu, U. and I. A. Svendsen (1992a). A mixing mechanism in the nearshore region. In *Proc. 23rd Int. Conf. Coastal Engng.*, Vol. 3, Venice, 2758–2771. ASCE.

Putrevu, U. and I. A. Svendsen (1992b). Shear instability of longshore currents: A numerical study. *J. Geophys. Res. 97*(C5), 7283–7303.

Sancho, F. E., I. A. Svendsen, J. Oltman-Shay, and E. B. Thornton (1997). Modelling nearshore circulation under field conditions. In *Proc. 3rd Int. Symp. WAVES97, Ocean Wave Measurement and Analysis*, Virginia Beach, 765–776. ASCE.

Sancho, F. E. P. and I. A. Svendsen (1997). Unsteady nearshore currents on longshore varying topographies. (Ph. D. Dissertation), Res. Report CACR-97-10, Center for Applied Coastal Research, Univ. of Delaware.

Shepard, F. P., K. O. Emery, and E. C. La Fond (1941). Rip currents: A process of geological importance. *J. Geology XLIX*(4), 337–369.

Slinn, D. N., J. S. Allen, P. A. Newberger, and R. A. Holman (1996). Nonlinear dynamics of alongshore currents over beaches with irregular topography. In *Proc. Amer. Geophys. Union, Fall Meeting*, S. Francisco, F388. AGU.

Sonu, C. J. (1972). Field observation of nearshore circulation and meandering currents. *J. Geophys. Res. 77*(18), 3232–3246.

Svendsen, I. A. (1984). Mass flux and undertow in a surf zone. *Coastal Engng. 8*, 347–365.

Svendsen, I. A. (1987). Analysis of surf zone turbulence. *J. Geophys. Res. 92*(C5), 5115–5124.

Thornton, E. B. and C. S. Kim (1993). Longshore current and wave height modulation at tidal frequency inside the surf zone. *J. Geophys. Res. 98*(C9), 16509–16519.

Van Dongeren, A. R., F. E. P. Sancho, I. A. Svendsen, and U. Putrevu (1994). Shorecirc: A quasi-3d nearshore model. In *Proc. 24th Int. Conf. Coastal Engng.*, Vol. 3, Kobe, 2741–2754. ASCE.

Van Dongeren, A. R. and I. A. Svendsen (1997). An absorbing-generating boundary condition for shallow water models. *J. of Waterway, Port, Coastal and Ocean Engng. 123*(6), 303–313.